Fractalkine (CX3CL1)– and Interleukin-2–Enriched Neuroblastoma Microenvironment Induces Eradication of Metastases Mediated by T Cells and Natural Killer Cells

Yan Zeng,[1] Nicole Huebener,[1] Stefan Fest,[1] Silke Weixler,[1] Ulrike Schroeder,[1] Gerhard Gaedicke,[1] Rong Xiang,[2] Alexander Schramm,[3] Angelika Eggert,[3] Ralph A. Reisfeld,[2] and Holger N. Lode[1]

[1]Pediatrics, Experimental Oncology, Charité Universitätsmedizin Berlin, Berlin, Germany; [2]Department of Immunology, The Scripps Research Institute, La Jolla, California; and [3]Department of Pediatric Hematology and Oncology, University of Essen, Essen, Germany

Abstract

Fractalkine (FKN) is a unique CX3C chemokine (CX3CL1) known to induce both adhesion and migration of leukocytes mediated by a membrane-bound and a soluble form, respectively. Its function is mediated through CX3C receptor (CX3CR), which is expressed by T_H1 immune cells including T cells and natural killer (NK) cells. FKN was shown to be expressed in >90% of 68 neuroblastoma samples as determined by cDNA microarray analysis. Here, we characterized the effect of FKN in the neuroblastoma microenvironment using a syngeneic model genetically engineered to secrete FKN. We show FKN-mediated migration, adhesion, and IFN-γ secretion of immune effector cells, but limited antineuroblastoma activity, *in vitro* and *in vivo*. Therefore, we tested the hypothesis that a combined increase of FKN and interleukin-2 (IL-2) in the neuroblastoma microenvironment induces an effective antitumor immune response. For this purpose, IL-2 was targeted to ganglioside GD2, which is highly expressed on neuroblastoma tissue, using an anti-GD2 antibody IL-2 immunocytokine (ch14.18-IL-2). Only mice bearing FKN- and IL-2–enriched neuroblastoma tumors exhibited a reduction in primary tumor growth and a complete eradication of experimental liver metastases. The depletion of T cells and NK cells *in vivo* abrogated the effect, and these effector cells showed the highest cytolytic activity *in vitro*. Finally, only the FKN- and IL-2–enriched neuroblastoma microenvironment resulted in T-cell activation and the release of proinflammatory cytokines. In summary, we showed for the first time the immunologic mechanisms by which targeted IL-2 treatment of neuroblastoma with an FKN-rich microenvironment induces an effective antitumor response. [Cancer Res 2007;67(5):2331–8]

Introduction

Development of an effective treatment against neuroblastoma is an important challenge in pediatric oncology. Neuroblastoma is the most common solid extracranial tumor in childhood. More than 50% of neuroblastoma patients initially present with disseminated stage IV disease characterized by dismal prognosis despite the introduction of novel therapeutic strategies such as high-dose chemotherapy followed by autologous blood stem cell transplantation and differentiation therapy with retinoic acid (1). One important prognostic factor in neuroblastoma associated with poor outcome is the amplification of the *MYCN* oncogene (2, 3), which is a well-established parameter used for treatment stratification. Although some of the cell biological implications of *MYCN* amplification on neuroblastoma growth, dissemination, and angiogenesis are understood, the role for immunotherapeutic approaches remains largely unknown. In a first report, the expression of chemokine CCL2 in neuroblastoma was found to inversely correlate with *MYCN* proto-oncogene amplification and *MYCN*-high/*CCL2*-low expression accurately predicted the absence of infiltrating natural killer (NK) T cells (4). This finding suggested for the first time a link between *MYCN* amplification and chemokine expression profile in neuroblastoma, with important implications for immunotherapy in this disease.

Immunotherapy in neuroblastoma currently under extensive clinical evaluation is targeting the ganglioside GD2 highly expressed in neuroblastoma tissue using ch14.18 and 3F8 monoclonal antibodies (mAb), as well as ch14.18-interleukin-2 (IL-2) fusion proteins (5, 6). These immunotherapies largely depend on the recruitment of immune effector cells to the neuroblastoma microenvironment, a mechanism primarily mediated by chemokines. The chemokine expression profile in neuroblastoma is not well characterized thus far. In microarray analyses, we found that the neuroblastoma microenvironment is characterized by the expression of tumor-associated chemokine fractalkine (FKN, CX3CL1), which is the sole member of the CX3C chemokine subfamily. The function of FKN is different from other chemokines related to its unique molecular structure. It exists in a soluble and a membrane-bound form, with the chemokine domain perched atop a long mucin-like stalk at the cell surface. Soluble FKN is released from the membrane following proteolytic cleavage mediated by disintegrin and metalloproteinases ADAM10 and ADAM17 [tumor necrosis factor-α (TNF-α) converting enzyme; ref. 7]. The FKN receptor CX3CR1 is specific for its ligand and not shared by other chemokines (8). The soluble and membrane-bound forms of FKN interact with CX3CR1 and thereby exert a dual function of inducing both leukocyte chemotaxis and adhesion (8–10). This is in contrast to CXC, CC, and C chemokines, which require additional molecules for leukocyte adhesion and migration, such as selectins and integrins. Furthermore, FKN is described to polarize T_H1 type immune responses, in contrast to the majority of chemokines found in cancer, which contribute to a T_H2 milieu (9) on the basis of the following characteristics. First, FKN activates mainly $CD16^+$

Requests for reprints: Holger N. Lode, Experimental Oncology, Charité Universitätsmedizin Berlin, Forum 4, R 2.0407, Augustenburger Platz 1, 13353 Berlin, Germany. Phone: 49-0-30-450-666-233; Fax: 49-0-30-450-559-917; E-mail: holger.lode@charite.de.

doi:10.1158/0008-5472.CAN-06-3041

NK cells, $CD8^+/CD3^+$ T cells, $CD4^+/CD3^+$ T cells, and $CD14^+$ monocytes, which all express the CX3CR1 receptor (10), and receptor expression is strongly up-regulated by IL-2 in both $CD4^+$ and $CD8^+$ T cells. Second, CX3CR1 is selectively expressed on various lineages of lymphocytes characterized by a high content of intracellular perforin and granzyme B, including NK cells, γδT cells, and terminally differentiated $CD8^+$ T cells (11), which are best equipped to eradicate malignant cells. Third, FKN was described to induce a T_H1 amplification circuit: FKN mRNA and protein expression is induced by IL-1, TNF-α, and IFN-γ, but not by IL-4 and IL-13, in human endothelial cells (11). In turn, soluble and membrane-bound FKN induce T_H1, but not T_H2, cytokine release from endothelial (12) and NK cells (13). Based on these considerations, the presence of FKN in the neuroblastoma microenvironment should provide for a T_H1 milieu and favor the efficacy of immunotherapy in this disease.

To provide for a model with increased amounts of FKN in the neuroblastoma microenvironment, we transferred the murine *FKN* gene into FKN-negative NXS2 murine neuroblastoma cells (13) to use them in syngeneic immunocompetent A/J mice. In this model, we first determined the effect of FKN on the neuroblastoma microenvironment and extended these findings by investigating efficacy and mechanisms of an immunotherapeutic strategy involving targeted IL-2, which already entered clinical evaluation for GD2-positive malignancies such as melanoma (14) and neuroblastoma (6).

The strategy of targeted IL-2 is based on the use of a tumor-specific antibody-cytokine fusion protein consisting of an anti–ganglioside GD2 antibody (ch14.18) fused to IL-2 (ch14.18-IL-2; ref. 15). This construct specifically directs IL-2 to ganglioside GD2, and it was shown in previous studies that ch14.18-IL-2 is effective against murine melanoma through activation and expansion of $CD8^+$ T cells (16). In a murine neuroblastoma model, in the absence of FKN in the tumor microenvironment, the ch14.18-IL-2 fusion protein also effectively eradicated established bone marrow metastasis (17). However, this effect was clearly and exclusively dependent on NK cells (18).

Here, we report expression of FKN in the neuroblastoma microenvironment of stage IV neuroblastoma patients. Because targeted IL-2 is currently under clinical evaluation in neuroblastoma patients (6), we investigated the effect of local FKN production on efficacy and mechanisms of targeted IL-2 therapy in a syngeneic model. For this purpose, murine FKN was cloned and expressed in the FKN-negative neuroblastoma cell line NXS2. The antitumor effect of FKN combined with targeted IL-2 was shown both for primary tumor growth and metastasis in syngeneic A/J mice. *In vivo* depletion of $CD4^+$, $CD8^+$ T cells and NK cells abrogated the therapeutic effect, suggesting that the main effector cells involved in the immunity were both T cells and NK cells. Up-regulation of T-cell activation markers and increased cytotoxicity elicited by T cells and NK cells further support the pivotal roles of T cells and NK cells in this immune response.

Materials and Methods

Cell culture and mice. NXS2 murine neuroblastoma cells syngeneic to A/J mice were grown as previously described (17). Syngeneic female A/J mice were obtained at 8 to 10 weeks of age from Harlan Winkelmann (Borchen, Germany). Animal experiments were done according to the German guide for the care and use of laboratory animals (i.e., "Tierschutzgesetz").

Determination of FKN expression in neuroblastoma patients. Expression of chemokines and their receptors was determined in 68 neuroblastoma patients by Affymetrix U95A array analysis. The patient cohort and data normalization procedures have been described elsewhere (19). *MYCN* status was determined by Southern blotting or fluorescence *in situ* hybridization by a reference laboratory as outlined in the German NB 97 protocol (20), and *MYCN* amplification is defined as >4-fold increase in *MYCN* copy number as defined by the ENQUA group (21) compared with the reference. Correlation of chemokine expression with molecular and clinical variables was determined using the stats package included in R2.2.[4] Visualization of gene expression was accomplished using Spotfire 8.1.

Cloning and expression of FKN. The cDNA of mFKN was cloned into pIRES vector (Clontech-Takara Bio Europe, Saint-Germain-en-Laye, France) by reverse transcription-PCR (pIRES-FKN) and transfected into NXS2 cells using Superfect (Qiagen, Hilden, Germany). Soluble mFKN was determined in cell culture supernatants from 10^6 NXS2 cells (wild-type, mock, and NXS2-FKN) after 24 h by sandwich ELISA (R&D Systems, Minneapolis, MN) according to the manufacturer's protocol. Membrane-bound mFKN was measured by flow cytometry. For this purpose, 10^6 parental cells (wild-type, mock, and NXS2-FKN) were incubated with goat anti-mouse FKN polyclonal antibody (clone M-18, Santa Cruz Biotechnology, Santa Cruz, CA; 1 μg/10^6 cells) and FITC-labeled anti-goat immunoglobulin G (IgG; Calbiochem, San Diego, CA) secondary antibody (10 μg/mL).

Migration assay. FKN-mediated migration was determined in Boyden chamber experiments (Costar Corp., Cambridge, MA). Splenocytes (2×10^5) were resuspended in 100 μL of serum-free RPMI medium and loaded on top of a 5-μm microporous transwell membrane in a 24-well plate. The bottom of the chamber contained the supernatants collected from NXS2-FKN cells. The migration was compared with serum-free medium and recombinant mFKN (R&D Systems) used as negative and positive controls, respectively. Transmigrated cells (6 h, 37°C, 5% CO_2) were counted in duplicate. To determine the specificity, functional blocking of FKN was done by adding anti-FKN antibody (M-18, Santa Cruz Biotechnology) into supernatants of FKN-producing NXS2 cells at a final concentration of 2 μg/mL and incubated for 1 h at 37°C before the migration assay.

Immunohistochemistry. Leukocytes in primary tumors were determined 3 weeks after s.c. inoculation of 2×10^6 NXS2 cells (wild-type, mock, and NXS2-FKN) in syngeneic A/J mice by immunohistochemistry. Tumor tissues were cryosectioned into 5-μm slides and stored at −20°C. Slides were blocked with 2.5% goat serum (Vector Laboratories, Burlingame, CA), incubated with 1.25 μg/mL rat anti-mouse CD4 (RM4-5), CD8 (53-6.7), or CD45 (30-F11; BD Biosciences PharMingen, San Diego, CA) primary antibodies followed by incubation with secondary biotin-labeled goat anti-rat IgG antibody (Calbiochem) and streptavidin-peroxidase (Elite ABC reagent, Vector Laboratories). Slides were analyzed by light microscopy, and quantification of infiltrating $CD4^+$, $CD8^+$, and $CD45^+$ cells was done by counting 10 fields at ×400 magnification.

Adhesion assay. NXS2 cells (wild-type, mock, and NXS2-FKN) were seeded at a density of 1×10^4 per well in a six-well plate to form a monolayer. Splenocytes were added at a density of 3×10^4 per well and cocultured overnight. After removal of nonadherent cells by PBS washing, the adherent cells were counted under a microscope in 10 high-power fields. Photos were taken at ×400 magnification.

IFN-γ secretion assay. Murine NK cells were isolated from splenocytes of A/J mice by immunomagnetic positive selection using antimouse pan NK cell antibody anti-CD49b (DX5) microbeads (Miltenyi Biotech GmbH, Bergisch-Gladbach, Germany) according to manufacturer's guidelines. The purity of cell fractions was determined by fluorescence-activated cell sorting (FACS) analysis. NXS2-FKN cells and control cells were seeded at a density of 1×10^4 per well and cocultured with 5×10^4 NK cells per well in 200-μL medium in a 96-well plate for 36 h. IFN-γ in the culture supernatants was measured by ELISA (BD Biosciences PharMingen).

[4] http://www.r-project.org

Tumor model. The effect of FKN and targeted IL-2 on neuroblastoma was determined in a murine neuroblastoma model (17). Briefly, NXS2 cells (wild-type, mock, and NXS2-FKN) were inoculated s.c. (2×10^6). Mice ($n = 6$) were treated with noncurative amounts of tumor-specific ch14.18-IL-2 (5 μg, i.v.) for 5 consecutive days. Results were compared with mice treated with ch225-IL-2, which were used as a nonspecific control. Local tumor growth was monitored for 16 days by microcaliper measurements and the tumor volume was calculated according to the following formula: volume = (length × width^2) / 2. One day after surgical removal of primary tumors (day 16), mice were challenged with wild-type NXS2 cells (1×10^5) and experimental liver metastases were determined 3 weeks after i.v. injection and scored by visually assessing the percentage of liver surface covered by fused metastases as follows: 0, 0%; 1, 20%; 2, 20% to 50%; 3, 50%.

***In vivo* depletion of CD4$^+$, CD8$^+$ T cells and NK cells.** T cells and NK cells were depleted using anti-CD4 (Gk1.5) and anti-CD8 (53-6.7) antibodies (BD PharMingen) or anti–asialo GM1 antisera (Wako Chemicals, Neuss, Germany) as previously described (18). Depletion of CD4$^+$, CD8$^+$ T cells or NK cells was accomplished by i.p. injection of anti-CD4 (200 μg), anti-CD8 (200 μg), or anti–asialo GM1 (50 μL) on days −1, 7, and 14.

Cytotoxicity assay. Cytotoxicity was determined in a standard ^{51}Cr release assay. Briefly, 2×10^6 NXS2 or yeast artificial chromosome-1 (YAC-1) target cells were labeled with 0.5 mCi sodium chromate Cr 51 (Perkin-Elmer, Wellesley, MA; 2 h, 37°C) and seeded into flat-bottomed 96-well plates (5,000/100 μL/well). Splenocytes were isolated from spleens under sterile conditions and cultured in RPMI (10% FCS, 100 μg/mL penicillin-streptomycin, 50 μmol/L β-Mercaptoethanol, 100 IU/mL IL-2) in the presence or absence of irradiated (50 Gy, 15 min) NXS2 neuroblastoma cells (1:100) for 4 days. Effector cells were added at various effector-to-target ratios in triplicates to a final volume of 200 μL/well. Supernatants were collected after incubation (6 h, 37°C 5% CO_2) and ^{51}Cr release was determined in a gamma counter (1470 WIZARD, Perkin-Elmer). Maximum release was induced with 10% SDS (10 μL/well). MHC class I restriction was determined by addition of anti–H-2K^k mAb (25 μg/mL, clone 36-7-5, BD PharMingen). Percent cytotoxicity was calculated as follows:

$$\%\text{lysis} = \frac{\text{experimental release[cpm]} - \text{maximum release[cpm]}}{\text{maximum release[cpm]} - \text{spontaneous release[cpm]}} \times 100$$

Flow cytometry. T-cell activation markers and intracellular cytokines were analyzed by flow cytometry. Freshly isolated splenocytes (10^6) were resuspendend in DMEM (10% FCS) and treated for 3 h with a cocktail of monensin (2 μmol/L), ionomycin (1 μg/mL), and phorbol 12-myristate 13-acetate (50 ng/mL; Sigma-Aldrich, Taufkirchen, Germany). Cells were fixed in PBS containing 1% paraformaldehyde (Sigma-Aldrich; 30 min, 4°C, dark). Cells were washed [1% bovine serum albumin, 0.1% sodium azide, PBS (pH 7.4)] and incubated (4°, 30 min) with antibodies directed against lymphocyte surface molecules (1:100): anti-CD3-FITC (145-2C11), anti-CD4-FITC (L3T4), anti-CD8-FITC (Ly-2), anti-CD4-phycoerythrin (Gk1.5), anti-CD8-phycoerythrin (53-6.7), anti-CD25-phycoerythrin (3C7), and anti-CD69-phycoerythrin (H1.2F3; BD PharMingen). Cells were washed and permeabilized (PBS, 0.1% saponin; Sigma-Aldrich). Intracellular cytokines were determined with anti-IFN-γ-phycoerythrin (XMG1.2) and anti-TNF-α-phycoerythrin (MP6-XT22) antibodies (1:200, 20 min, 4°C, dark; BD PharMingen). Samples were analyzed using a FACSCalibur (Becton Dickinson, Germany) equipped with CellQuest.

Statistics. The statistical significance of differential findings of *in vitro* assays and between liver weights of experimental groups of animals was determined by two-tailed Student's t test. The differential findings of hepatic metastasis scores of liver metastases between experimental groups were determined by the nonparametric Mann-Whitney U test. Findings were regarded as significant if two-tailed $P < 0.05$.

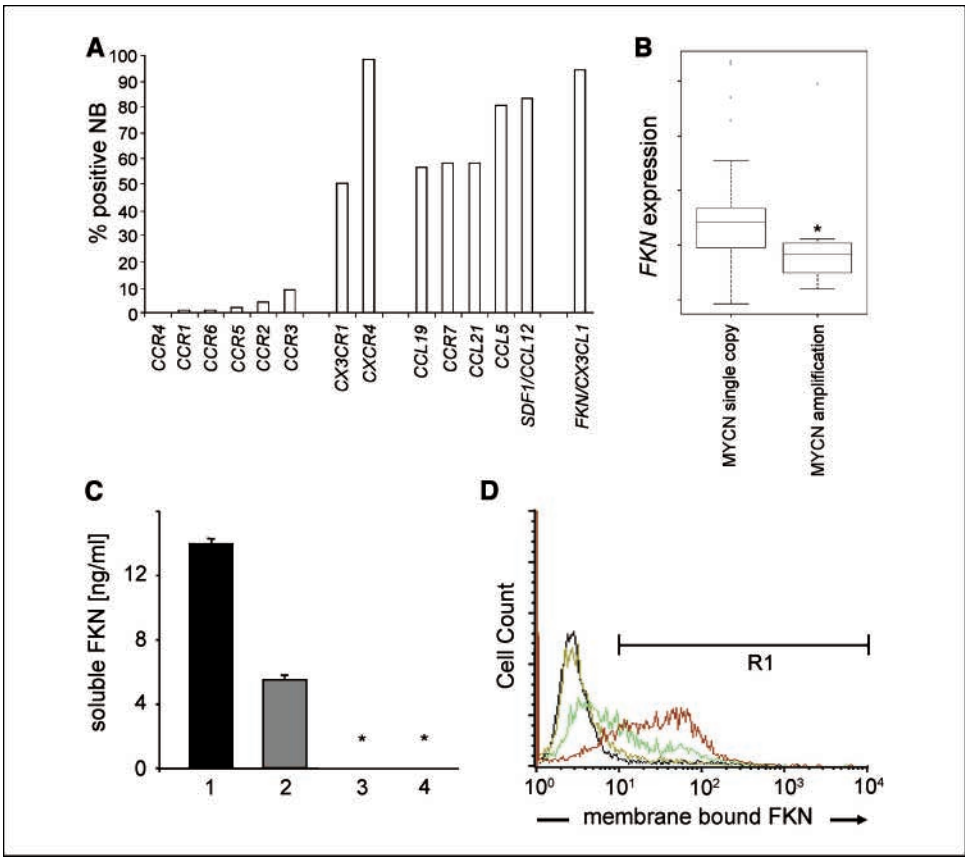

Figure 1. Expression of *FKN* in neuroblastoma. The gene expression of chemokines and chemokine receptors was determined in 68 human neuroblastoma (*NB*) samples (*A*) and correlated with the expression of *MYCN* oncogene in these tumors (*B*). *A,* results indicate expression of chemokines in the majority of neuroblastomas and the presence of *FKN* (*CX3CL1*), as well as *SDF1*, in almost all of the tumors investigated. Expression of chemokine receptors was virtually absent in neuroblastoma samples analyzed here, with exception of the FKN receptors *CX3CR1* and *CXCR4. B,* the amplification of *MYCN* in these tumor samples inversely correlated with the expression of the *FKN* gene as shown by box plots of *MYCN* amplification and *FKN* gene expression (*, $P < 0.05$, t test). Expression of the FKN protein by NXS2 cells as secreted (*C*) and membrane-bound (*D*) protein was determined by sandwich ELISA and flow cytometry, respectively. *C, columns,* mean FKN secretion rates (ng/mL/24 h) obtained from triplicate experiments; *bars,* SD. *1,* NXS2-FKN (third-generation subclone); *2,* NXS2-FKN bulk culture; *3,* NXS2 mock-transfected cells; *4,* NXS2 parental cells. *Asterisks,* nondetectable levels of FKN. *D,* the presence of the membrane-bound FKN protein was quantified by flow cytometry. *Black,* NXS2 wild-type cells; *yellow,* NXS2 mock-transfected cells; *green,* NXS2-FKN bulk culture; *red,* NXS2-FKN third-generation subclone.

Results

Expression of FKN in neuroblastoma tumor tissue. The gene expression profile of chemokines and their receptors was obtained from 68 primary neuroblastoma samples by Affymetrix U95A microarray analyses. Results show that most of the known chemokine genes are expressed, whereas the chemokine receptor genes *CCR1* to *CCR6* are not expressed. Chemokine receptor genes *CCR7* and *CXCR4* could be detected in 58% and 98% of tumor samples, respectively. Interestingly, the chemokine gene *FKN* (*CX3CL1*) was also expressed in all but two samples (Fig. 1*A*) and exhibited an unusual expression pattern when compared with the other members of the chemokine family. Based on a previously reported inverse correlation of *CCL2* gene expression and *MYCN* amplification in neuroblastoma (4) and the abundant gene expression of the *FKN* gene observed in our set of samples (Fig. 1*A*), we investigated the relation of *MYCN* amplification and *FKN* gene expression. Interestingly, we also found that the *FKN* gene expression was anti-correlated to *MYCN* amplification (Fig. 1*B*). Based on these findings, we investigated the role of FKN in the neuroblastoma microenvironment for immunotherapy in a syngeneic model of neuroblastoma.

Expression and function of FKN produced by NXS2 neuroblastoma cells. The expression of the FKN protein in the secreted and membrane-bound form was assessed after *FKN* gene transfer into NXS2 neuroblastoma cells (Fig. 1*C* and *D*). In FKN-NXS2 bulk culture cells, the level of the soluble form of FKN was quantified at a rate of 5.5 ± 0.48 ng/mL/24 h, and flow cytometry analysis revealed that 31% of these cells expressed the membrane-bound form of FKN. After two rounds of subcloning, a NXS2-FKN subclone was established, characterized by a higher FKN secretion rate of 14 ± 1.0 ng/mL/24 h with 75% of the cells expressing FKN bound to the cell surface. This NXS2-FKN subclone was selected for further *in vitro* and *in vivo* studies referred to as NXS2-FKN from here on.

Chemotaxis mediated by supernatants from NXS2-FKN cells containing 47.6 ng/mL FKN was tested in a Boyden chamber, which revealed a maximum of 25% to 30% of migrated cells (Fig. 2*A*), in contrast to the negative control (3%). Chemotaxis was partially blocked by adding antimurine FKN.

Antibodies (2 μg/mL) were added into supernatants to indicate that migration was specifically mediated by FKN in this assay. Interestingly, migration including recombinant FKN, which served as a positive control, showed a "bell-shaped" distribution with a decrease at higher concentration, a known but not well-understood characteristic phenomenon in chemotaxis experiments.

To determine FKN-mediated chemotaxis *in vivo*, the infiltration of leukocytes into primary tumors ($n = 6$) 16 days after s.c. injection of 2×10^6 NXS2-FKN, NXS2-mock, and NXS2 parental cells was analyzed by immunohistochemistry (Fig. 2*B* and *C*). Effective infiltration by leukocytes into FKN-producing primary tumors was clearly shown, indicated by an increase by a factor of 3 over the NXS2 wild-type and mock-transfected controls. Interestingly, the highest increase in migration by a factor of 7 was observed in the $CD8^+$ T-cell subpopulation (Fig. 2*B* and *C*). The biofunction of the membrane-bound form of FKN was determined *in vitro* by analysis of FKN-mediated cell-cell adhesion of leukocytes to NXS2-FKN cells (Fig. 3*A* and *B*). For this purpose, NXS2-FKN cells and

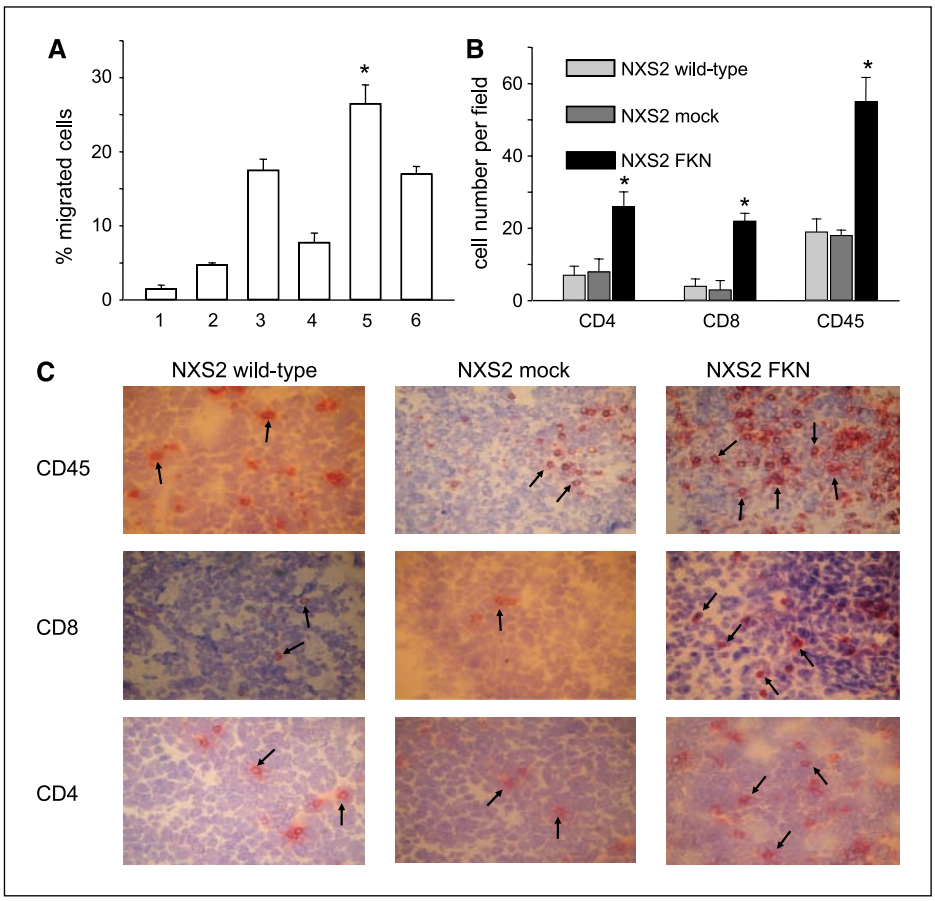

Figure 2. FKN-mediated chemotaxis. Chemotactic activity of FKN was determined both *in vivo* and *in vitro*. *A,* FKN-mediated chemotaxis was assessed in a Boyden chamber assay *in vitro*. The total number of transmigrated cells was determined microscopically. *Columns,* mean percent of transmigrated cells from triplicate experiments; *bars,* SD. *1,* serum-free NXS2-mock supernatant (negative control); *2,* recombinant murine FKN 12.5 ng/mL; *3,* 20 ng/mL; *4,* 50 ng/mL; *5,* serum-free NXS2-FKN supernatant; *6,* serum-free NXS2-FKN supernatant plus 2 μg/mL anti-mFKN mAb (M18), indicating that there is an additional migration-inducing bioactivity in the supernatant equivalent to 20 ng/mL FKN, assuming 100% efficiency of blockade by the mFKN mAb. *, $P < 0.01$, experimental groups versus control groups. *B* and *C,* cryosections of primary tumors induced with NXS2 cells (wild-type, mock, and NXS2-FKN) were stained with mAbs specific for CD45 (pan leukocyte marker) and for CD4 and CD8 (T-cell subpopulations). *B,* number of tumor infiltrating cells quantified by counting the total number of infiltrating cells per high-power field at ×400. *Columns,* mean of 10 high-power fields; *bars,* SD. *, $P < 0.01$, between mice receiving NXS2-FKN cells and all control groups. *C,* photographs of representative areas within distinct primary tumors (×400). *Black arrows,* infiltrating cells with characteristic red membrane staining.

control cells were incubated with splenocytes. NXS2-FKN induced a 3.2-fold increase of adherent splenocytes compared with NXS2 control cells (wild-type and mock), suggesting that FKN bound to neuroblastoma cell membranes mediated firm adhesion of splenocytes. Finally, we analyzed the release of IFN-γ by NK cells induced by NXS2-FKN. For this purpose, NK cells were enriched to a purity of 90% as determined by FACS analysis with anti-CD49b (DX5) mAb (data not shown). The highest amount of IFN-γ was observed in the supernatant of NK cells cocultured with NXS2-FKN cells (254 ± 133 pg/mL; mean ± SD; Fig. 3*C*), in contrast to NXS2 wild-type (ND) and NXS2 mock controls (42 ± 19 pg/mL). This finding is consistent with reports suggesting an autocrine amplification loop of NK cell activation (22–24), emphasizing the important role of FKN in induction of a T_H1 tumor microenvironment.

Effect of targeted IL-2 on the FKN-rich neuroblastoma microenvironment. The effect of targeted IL-2 on neuroblastoma producing FKN was first evaluated on primary tumor growth. The presence of FKN in primary tumors induced by s.c. injection of NXS2-FKN cells resulted in a limited decrease of the average primary tumor growth rate (Fig. 4*A*). This finding was in contrast to mice treated with a small noncurative amount of ch14.18-IL-2 (5 × 5 μg i.v. on consecutive days starting 5 days after tumor cell inoculation), which resulted in a marked reduction of primary tumor growth (Fig. 4*A*). Importantly, one third (two of six) of mice showed a complete tumor rejection in this group (data not shown). At this point, it is important to note that the treatment of established NXS2 neuroblastoma tumors with ch14.18-IL-2 in the absence of FKN in the microenvironment (5 × 5 μg i.v. on consecutive days starting 5 days after tumor cell inoculation) was shown to be ineffective in several reports (25, 26). The effect of ch14.18-IL-2 on the FKN-rich neuroblastoma microenvironment was specific because the nonspecific control, ch225-IL-2, had no effect, as indicated by an average tumor size of 297.7 ± 35.1 mm^3 in the ch225-IL-2 group. This finding is not different from the average tumor size of the FKN-rich neuroblastoma microenvironment (315.3 ± 67.3 mm^3; $P > 0.1$).

The efficacy of ch14.18-IL-2 therapy of the FKN-rich neuroblastoma translated into protective immunity against liver metastasis following a lethal i.v. challenge with 10^5 wild-type NXS2 cells. Importantly, all mice challenged with NXS2 wild-type cells receiving the FKN and ch14.18-IL-2 combination therapy were free of liver metastasis (Fig. 4*C*) and livers of mice in this group revealed a normal weight (Fig. 4*B*), which is ~1 g.

Mechanisms involved in FKN-dependent anti-neuroblastoma activity of targeted IL-2. To elucidate effector cells involved in FKN-dependent antineuroblastoma activity of targeted IL-2, mice were depleted of $CD4^+$, $CD8^+$ T cells and NK cells (Fig. 5). Depletion of $CD8^+$ T cells resulted in abrogation of the antitumor effect, in contrast to the depletion of $CD4^+$ T cells, which was less effective, suggesting a helper function of this T-cell subpopulation. In NK cell–depleted mice, primary tumor growth rate was also accelerated, in contrast to nondepleted controls, indicating the involvement of NK cells. Thus, the antitumor effect of ch14.18-IL-2 in the FKN-producing neuroblastoma microenvironment is orchestrated by both T cells and NK cells with a predominant role for $CD8^+$ T cells. This contention was supported by the analysis of tumor-specific cytolytic activity and T-cell activation markers (Fig. 6). Splenocytes from mice with a FKN-rich tumor microenvironment treated with ch14.18-IL-2 revealed a 2-fold increase of the cytolytic response against

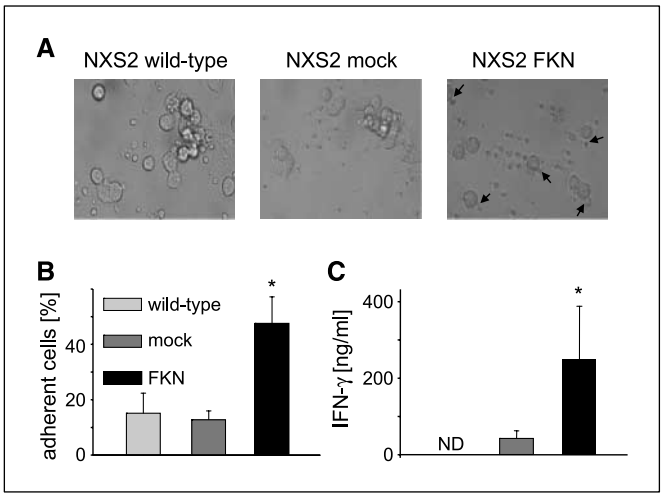

Figure 3. Leukocyte adhesion and secretion of IFN-γ induced by FKN. Adhesion induced by the membrane-bound form of FKN was determined by coincubation of splenocytes and NXS2-FKN cells. *A,* adhesion between NXS2-FKN cells and splenocytes after 12 h of incubation. Pictures were taken at ×400. *Arrows,* splenocytes adherent to NXS2-FKN cells. *B,* the percentage of splenocytes adherent to NXS2 cells (wild-type, mock, and NXS2-FKN) was determined by counting 10 high-power fields. *, $P < 0.01$, between NXS2-FKN cells and all control groups. *C,* secretion of IFN-γ from NK cells was determined by coincubation of NK cells with NXS2 cells (wild-type, mock, and NXS2-FKN) for 36 h. IFN-γ was measured in culture supernatant by ELISA. *Columns,* mean of triplicate cultures; *bars,* SD. *ND,* nondetectable. *, $P < 0.05$, between NXS2-FKN cells and all control groups.

NXS2 cells, in contrast to the mock control group (Fig. 6*A*). This NXS2 target cell lysis was inhibited by addition of anti–MHC class I ($H\text{-}2K^k$) antibody (Fig. 6*A*), indicating MHC class I restriction, a characteristic of a $CD8^+$ T-cell–mediated immune response. Importantly, no NXS2 lysis was observed with control splenocytes from mice with a FKN-rich microenvironment in the presence and absence of ch225-IL-2, which was used as a nonspecific control (Fig. 6*A*), again showing specificity and effective targeting of IL-2 following ch14.18-IL-2 therapy. The absent activation of T cells in the FKN-rich neuroblastoma microenvironment is in contrast to findings in the NK cell compartment. Here, the presence of FKN in the neuroblastoma microenvironment resulted in NK cell activation, as indicated by a cytolytic activity of splenocytes against YAC-1 cells in the 30% range (Fig. 6*B*). This activation was further amplified following therapy with ch14.18-IL-2 but not with ch225-IL-2.

Finally, we determined the level of T-cell activation as indicated by the expression of T-cell activation markers (CD25, CD69) and the production of proinflammatory cytokines (TNF-α, IFN-γ) by distinct T-cell populations (CD4, CD8; Fig. 6*C*). Importantly, the highest increase in all variables investigated indicating T-cell activation was observed in mice with a FKN-rich neuroblastoma microenvironment treated with ch14.18-IL-2 compared with all control groups including mice treated with the nonspecific ch225-IL-2 fusion protein. In summary, these findings show the induction of a $CD8^+$ T-cell–mediated immune response only in the presence of FKN and IL-2 in the neuroblastoma microenvironment.

Discussion

A complex network of chemokines plays an important role in the development of malignant disease by regulation of angiogenesis

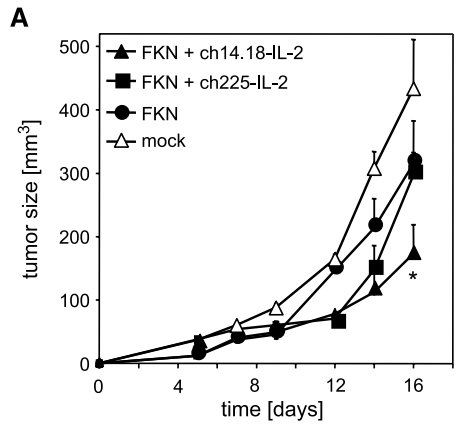

C

Treatment group	Metastases
mock	3,3,3,3,3,3
FKN	2,2,1,1,0,0
FKN + ch225-IL-2	2,1,1,1,0,0
FKN + ch14.18-IL-2	0,0,0,0,0,0*

Figure 4. Antitumor effect of targeted IL-2 against neuroblastoma expressing FKN. Antitumor effects of IL-2 targeted to the GD2-positive neuroblastoma microenvironment expressing FKN was determined on primary tumors (*A*) and liver metastases (*B* and *C*). Mice ($n = 6$) were inoculated s.c. with 2×10^6 NXS2 cells (mock and NXS2-FKN). Treatment with noncurative doses (5×5 μg i.v.) of targeted IL-2 (ch14.18-IL-2) and nonspecific control (ch225-IL-2) was started on day 5. *A,* primary tumor growth was monitored over time by microcaliper measurements. *, $P < 0.05$, between mice receiving ch14.18-IL-2 and all control groups. One day after removal of primary tumors (day 18), mice received a lethal challenge of NXS2 wild-type cells (1×10^5, i.v.; *B* and *C*). After 3 wk, liver metastasis was determined by assessment of the percentage of liver surfaces covered by fused metastases (*C*) and by measuring liver weights (*B*). *Points,* mean; *bars,* SD. *, $P < 0.05$, between the group of mice treated with ch14.18-IL-2 and all control groups.

and metastasis, control of leukocyte trafficking into the tumor microenvironment, and modulation of host antitumor immune responses (8). Within this network, FKN (neurotactin, CX3CL1) attracted the attention of tumor immunologists based on its unique dual function of inducing both leukocyte adhesion and migration and providing for a T_H1 milieu once expressed in the tumor microenvironment. We confirmed these functional aspects of FKN and showed the presence of FKN in soluble and membrane-bound forms mediating migration and adhesion of leukocytes, as well as induction of T_H1 cytokine IFN-γ (Figs. 1–3). It was reported that FKN can stimulate the expression of IFN-γ, which in turn enhances the expression of FKN by endothelial cells, indicating a paracrine amplification loop (22, 23), consistent with a marked increase of IFN-γ expression in cocultures of NK cells with FKN-expressing NXS2 cells (Fig. 3).

Based on these considerations and based on the observation of FKN expression in tumor tissue of neuroblastoma patients (Fig. 1), we tested the effect of FKN production in the microenvironment of NXS2 neuroblastoma primary tumors on the induction of tumor protective immunity. In similar studies, *FKN* gene transfer was investigated in a limited number of animal models thus far, including lung carcinoma (24, 27), colon carcinoma (24, 28), and melanoma (28). In all these studies, FKN was effective in inducting an antitumor response mediated by both NK and T cells. These findings are in contrast to results reported here because the expression of FKN in the NXS2 neuroblastoma microenvironment resulted in limited efficacy, as indicated by a reduction of primary tumor growth by only 30% (Fig. 4*A*). Such observations were also made in an ovarian carcinoma model, in which FKN was ineffective in suppressing tumor growth despite accumulation of T cells and NK cells in the tumor microenvironment (27). The explanation provided for the ovarian carcinoma model was a proangiogenic property of FKN possibly masking its tumor suppressive activity. This argument can be challenged because FKN induces the release of IFN-γ, leading to the secretion of antiangiogenic chemokines (e.g., IFN-inducible protein 10), a phenomenon described as immunoangiostasis (29). Therefore, the exact role of FKN in angiogenesis needs further investigation. Based on the limited level of T-cell activation observed in our model with FKN-rich neuroblastoma tumors, in the absence of targeted IL-2 therapy (Fig. 6), we favor a skewed balance toward the release of anti-inflammatory factors from NXS2 cells such as IL-10 and transforming growth factor-β, both produced in large amounts by NXS2 cells (data not shown), as an explanation for the poor antitumor response.

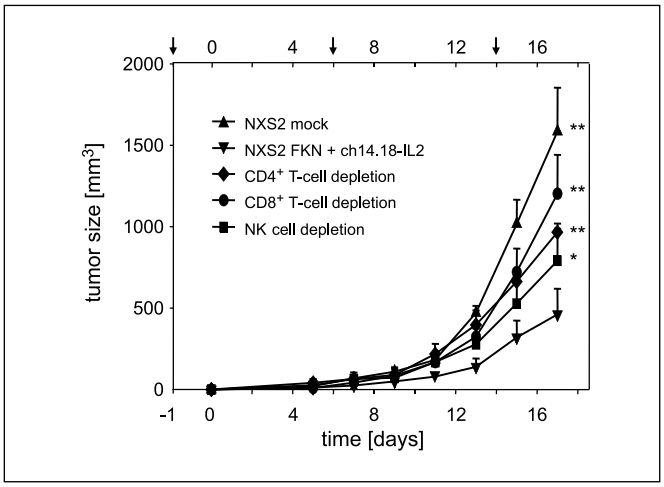

Figure 5. Effect of T-cell and NK cell depletion on targeted IL-2 therapy of FKN-expressing neuroblastoma. Mice ($n = 6$) were inoculated s.c. with 2×10^6 NXS2 cells (mock and NXS2-FKN) and treatment with noncurative doses (5×5 μg i.v.) of targeted IL-2 (ch14.18-IL-2) was started on day 5. *In vivo* depletion of $CD4^+$ and $CD8^+$ T cells, as well as NK cells, during the effector phase was accomplished as described. *Arrows,* time points of *in vivo* depletion. Primary tumor growth was monitored over time by microcaliper measurements. *Points,* mean; *bars,* SD. *, $P < 0.05$; **, $P < 0.01$, between the nondepleted group and all control groups.

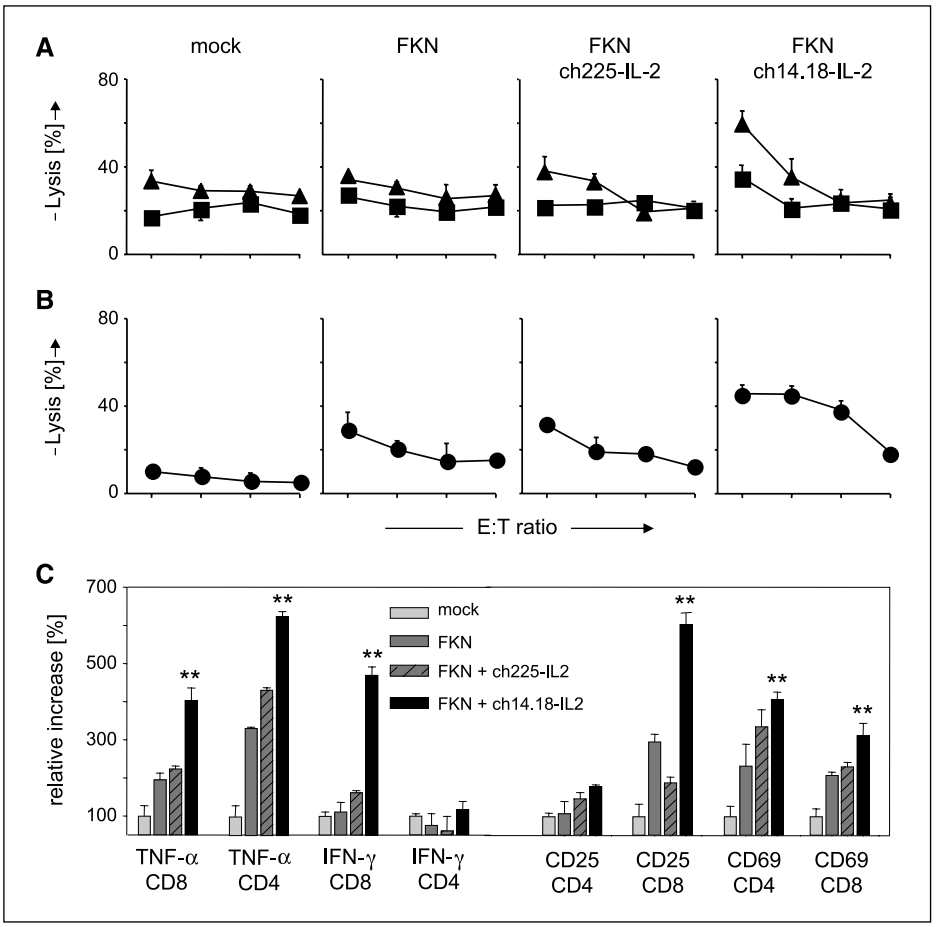

Figure 6. T-cell activation and cytolytic response following ch14.18-IL-2 therapy of neuroblastoma expressing FKN. Splenocytes were isolated from mice bearing FKN-producing neuroblastoma tumors treated with specific ch14.18-IL-2 and nonspecific ch225-IL-2 as described in Fig. 5 and subjected to *in vitro* stimulation (4 d, 50 Gy irradiated NXS2 wild-type). *A* and *B,* cytotoxicity was determined by ^{51}Cr release assay at varying effector-to-target (*E:T*) ratios (left to right: 200:1, 100:1, 50:1, and 25:1). MHC class I–restricted lysis (*A*) was determined in the absence (▲) and presence (■) of anti–MHC class I antibody (anti–H-2K^k, 25 μg/mL). Cytolytic response induced by NK cells (*B*) was measured with YAC-1 target cells. *Points,* mean of triplicate experiments; *bars,* SD. Error bars not displayed are covered by symbols. *C,* intracellular cytokine production (IFN-γ, TNF-α) and the expression of T-cell activation markers (CD25, CD69) by T-cell subpopulations (CD4, CD8) were determined by two-color flow cytometry. *Columns,* mean percent relative increase over naïve control splenocytes obtained in triplicate experiments; *bars,* SD. **, $P < 0.01$, between the group of mice treated with ch14.18-IL-2 and control groups.

To activate leukocytes attracted by FKN produced in the tumor microenvironment, mice were treated with small noncurative amounts of an anti–disialo-ganglioside GD2-IL-2 fusion protein (ch14.18-IL-2). This fusion protein directs IL-2 into the GD2-positive tumor microenvironment. The combination strategy resulted in significant inhibition of primary tumor growth (Fig. 4), and one third of mice revealed primary tumor rejection. Furthermore, all of these mice were completely free of experimental liver metastasis, showing systemic immunity against lethal wild-type NXS2 cell challenges.

The immune response involved in FKN-dependent anti-neuroblastoma activity of targeted IL-2 revealed a predominant role for $CD8^+$ T cells as indicated by the following lines of evidence. First, depletion of $CD8^+$ T cells was more effective in abrogation of the antitumor effect than depletion of NK cells and $CD4^+$ T cells (Fig. 5), suggesting a crucial role for $CD8^+$ T cells. Second, MHC class ^{2}–restricted NXS2 target cell killing, characteristic for $CD8^+$ T cells, was only increased in splenocytes of mice with a FKN-rich tumor microenvironment treated with targeted IL-2 (Fig. 6). Interestingly, the FKN-rich tumor microenvironment resulted in NK cell activation as indicated by an increased YAC-1 target cell lysis up to 30% (Fig. 6). However, this effect did not translate into a reduction of primary tumor growth (Fig. 4), supporting the crucial role for recruiting $CD8^+$ T cells for effective antitumor immune responses. Targeted IL-2 boosted FKN-dependent NK cell–mediated YAC-1 target cell lysis from 30% to up to 50%, suggesting an important bystander effect of NK cells. Third, the highest degree of T-cell activation, as indicated by an up-regulation of T-cell activation markers (CD25, CD69) and production of T_H1 type cytokines (TNF-α, IFN-γ), was found in mice with a FKN-rich tumor microenvironment treated with targeted IL-2.

The induction of a $CD8^+$ T-cell–mediated immune response following targeted IL-2 into a FKN-rich neuroblastoma is in contrast to results observed with targeted IL-2 into a FKN-low neuroblastoma microenvironment. In the FKN-low neuroblastoma microenvironment, targeted IL-2 was effective using ch14.18-IL-2 at higher doses (5 × 20 μg i.v.) in the same animal model (18). However, the antitumor effect was exclusively mediated by NK cells, not by $CD8^+$ T cells, as indicated by the absence of primary tumor infiltration by T cells ($CD4^+$, $CD8^+$), by the lack of a MHC class I–restricted NXS2 target cell lysis, and by a persistent therapeutic effect in mice depleted of $CD8^+$ T cells. Therefore, these findings suggest that the presence of FKN in the neuroblastoma microenvironment may provide for a shift from innate to adaptive immunity following targeted IL-2 therapy. This has important implications for immunologic monitoring of neuroblastoma patients treated with targeted IL-2. The correlation of low N-*myc* copy number with increased FKN (Fig. 1) and CCL2 expression (4) in neuroblastoma tissue suggests that such patients may present with a T-cell– or NK T-cell–mediated antineuroblastoma response on treatment with targeted IL-2. This is in contrast to patients with N-*myc*–amplified neuroblastoma, an issue that needs to be addressed in clinical studies. This contention is further supported by the possibility of increasing the generally low MHC class I expression in neuroblastoma by FKN-mediated induction of IFN-γ. However, additional studies are required to determine this modulation of MHC class I antigen expression.

In summary, we showed for the first time that the immune response following targeted IL-2 therapy largely depends qualitatively and quantitatively on the presence of FKN in the neuroblastoma microenvironment. This effect was mediated by recruitment of $CD8^+$ effector T cells to induce an antitumor response best equipped to further improve the outcome following adjuvant treatment of patients with minimal residual disease.

Acknowledgments

Received 8/16/2006; revised 10/30/2006; accepted 12/22/2006.

Grant support: Deutsche Forschungsgemeinschaft grant Lo 635 (H.N. Lode and Y. Zeng), Fördergesellschaft Kinderkrebs-Neuroblastom Forschung e.V. (H.N. Lode and S. Weixler), and a training grant from the Charité (S. Fest).

The costs of publication of this article were defrayed in part by the payment of page charges. This article must therefore be hereby marked *advertisement* in accordance with 18 U.S.C. Section 1734 solely to indicate this fact.

We thank Anne Strandsby for technical assistance.

References

1. Matthay KK, Villablanca JG, Seeger RC, et al. Treatment of high-risk neuroblastoma with intensive chemotherapy, radiotherapy, autologous bone marrow transplantation, and 13-*cis*-retinoic acid. Children's Cancer Group. N Engl J Med 1999;341:1165–73.
2. Seeger RC, Brodeur GM, Sather H, et al. Association of multiple copies of the N-myc oncogene with rapid progression of neuroblastomas. N Engl J Med 1985;313:1111–6.
3. Brodeur GM, Seeger RC, Schwab M, Varmus HE, Bishop JM. Amplification of N-myc in untreated human neuroblastomas correlates with advanced disease stage. Science 1984;224:1121–4.
4. Metelitsa LS, Wu HW, Wang H, et al. Natural killer T cells infiltrate neuroblastomas expressing the chemokine CCL2. J Exp Med 2004;199:1213–21.
5. Zeng Y, Fest S, Kunert R, et al. Anti-neuroblastoma effect of ch14.18 antibody produced in CHO cells is mediated by NK-cells in mice. Mol Immunol 2005;42:1311–9.
6. Osenga KL, Hank JA, Albertini MR, et al. A phase I clinical trial of the hu14.18-IL2 (EMD 273063) as a treatment for children with refractory or recurrent neuroblastoma and melanoma: a study of the Children's Oncology Group. Clin Cancer Res 2006;12:1750–9.
7. Hundhausen C, Misztela D, Berkhout TA, et al. The disintegrin-like metalloproteinase ADAM10 is involved in constitutive cleavage of CX3CL1 (fractalkine) and regulates CX3CL1-mediated cell-cell adhesion. Blood 2003;102:1186–95.
8. Balkwill F. Cancer and the chemokine network. Nat Rev Cancer 2004;4:540–50.
9. Imai T, Hieshima K, Haskell C, et al. Identification and molecular characterization of fractalkine receptor CX3CR1, which mediates both leukocyte migration and adhesion. Cell 1997;91:521–30.
10. Nishimura M, Umehara H, Nakayama T, et al. Dual functions of fractalkine/CX3C ligand 1 in trafficking of perforin+/granzyme B+ cytotoxic effector lymphocytes that are defined by CX3CR1 expression. J Immunol 2002;168:6173–80.
11. Fraticelli P, Sironi M, Bianchi G, et al. Fractalkine (CX3CL1) as an amplification circuit of polarized Th1 responses. J Clin Invest 2001;107:1173–81.
12. Yoneda O, Imai T, Nishimura M, et al. Membrane-bound form of fractalkine induces IFN-γ production by NK cells. Eur J Immunol 2003;33:53–8.
13. Zeng Y, Jiang J, Huebener N, et al. Fractalkine gene therapy for neuroblastoma is more effective in combination with targeted IL-2. Cancer Lett 2005;228:187–93.
14. King DM, Albertini MR, Schalch H, et al. Phase I clinical trial of the immunocytokine EMD 273063 in melanoma patients. J Clin Oncol 2004;22:4463–73.
15. Lode HN, Xiang R, Becker JC, Gillies SD, Reisfeld RA. Immunocytokines: a promising approach to cancer immunotherapy. Pharmacol Ther 1998;80:277–92.
16. Becker JC, Pancook JD, Gillies SD, Furukawa K, Reisfeld RA. T cell-mediated eradication of murine metastatic melanoma induced by targeted interleukin 2 therapy. J Exp Med 1996;183:2361–6.
17. Lode HN, Xiang R, Varki NM, et al. Targeted interleukin-2 therapy for spontaneous neuroblastoma metastases to bone marrow. J Natl Cancer Inst 1997;89:1586–94.
18. Lode HN, Xiang R, Dreier T, et al. Natural killer cell-mediated eradication of neuroblastoma metastases to bone marrow by targeted interleukin-2 therapy. Blood 1998;91:1706–15.
19. Schramm A, Schulte JH, Klein-Hitpass L, et al. Prediction of clinical outcome and biological characterization of neuroblastoma by expression profiling. Oncogene 2005;24:7902–12.
20. Weber A, Imisch P, Bergmann E, Christiansen H. Coamplification of DDX1 correlates with an improved survival probability in children with MYCN-amplified human neuroblastoma. J Clin Oncol 2004;22:2681–90.
21. Ambros IM, Benard J, Boavida M, et al. Quality assessment of genetic markers used for therapy stratification. J Clin Oncol 2003;21:2077–84.
22. Guo J, Zhang M, Wang B, et al. Fractalkine transgene induces T-cell-dependent antitumor immunity through chemoattraction and activation of dendritic cells. Int J Cancer 2003;103:212–20.
23. Guo J, Chen T, Wang B, et al. Chemoattraction, adhesion and activation of natural killer cells are involved in the antitumor immune response induced by fractalkine/CX3CL1. Immunol Lett 2003;89:1–7.
24. Xin H, Kikuchi T, Andarini S, et al. Antitumor immune response by CX3CL1 fractalkine gene transfer depends on both NK and T cells. Eur J Immunol 2005;35:1371–80.
25. Lode HN, Moehler T, Xiang R, et al. Synergy between an antiangiogenic integrin αv antagonist and an antibody-cytokine fusion protein eradicates spontaneous tumor metastases. Proc Nat Acad Sci U S A 1999;96:1591–6.
26. Lode HN, Xiang R, Duncan SR, et al. Tumor-targeted IL-2 amplifies T cell-mediated immune response induced by gene therapy with single-chain IL-12. Proc Natl Acad Sci U S A 1999;96:8591–6.
27. Gao JQ, Tsuda Y, Katayama K, et al. Antitumor effect by interleukin-11 receptor α-locus chemokine/CCL27, introduced into tumor cells through a recombinant adenovirus vector. Cancer Res 2003;63:4420–5.
28. Nukiwa M, Andarini S, Zaini J, et al. Dendritic cells modified to express fractalkine/CX3CL1 in the treatment of preexisting tumors. Eur J Immunol 2006;36:1019–27.
29. Strieter RM, Belperio JA, Burdick MD, et al. CXC chemokines: angiogenesis, immunoangiostasis, and metastases in lung cancer. Ann N Y Acad Sci 2004;1028:351–60.

Fractalkine (CX3CL1)– and Interleukin-2–Enriched Neuroblastoma Microenvironment Induces Eradication of Metastases Mediated by T Cells and Natural Killer Cells

Yan Zeng, Nicole Huebener, Stefan Fest, et al.

Cancer Res 2007;67:2331-2338.